Yuriy Plevachuk[a], Stepan Mudry[a], Vasyl Sklyarchuk[a], Andriy Yakymovych[a], Andriy Korolyshyn[a], Ihor Shtablavyy[a], Yuriy Kulyk[a], Ulrich E. Klotz[c], Chunlei Liu[b,d], Christian Leinenbach[b]

[a] Ivan Franko National University, Department of Metal Physics, Lviv, Ukraine
[b] Empa, Swiss Federal Laboratories for Materials Testing and Research, Laboratory of Joining & Interface Technology, Dübendorf, Switzerland
[c] FEM, Research Institute Precious Metals & Metals Chemistry, Schwäbisch Gmünd, Germany
[d] Now at: ABB Research Center, Baden-Dättwil, Switzerland

Determination of liquidus temperature in Sn–Ti–Zr alloys by viscosity, electrical conductivity and XRD measurements

The Sn–Ti–Zr system is an important subsystem for Cu based active brazing filler metals. Experimental results on this system, however, are rather scarce. The diagram is rather uncertain regarding most of the liquidus, especially on the Sn rich side. In this work, the atomic structure and temperature dependence of structure-sensitive physical properties (dynamic viscosity and electrical conductivity) of liquid Sn–Ti–Zr alloys in the Sn-rich corner were investigated in a wide temperature range with special attention to the melting–solidification region. The results allowed the liquidus line position to be specified.

Keywords: Sn–Ti–Zr; Phase diagrams; Viscosity; Electrical conductivity; XRD

1. Introduction

Filler metals for diamond brazing are usually based on ternary or quaternary Cu- and Sn-based systems such as Cu–Sn–Ti–Zr which contain active elements such as Ti or Zr in order to wet the diamond or other ceramic materials. Very accurate information on physical properties, thermodynamic data and phase diagrams of all the binary and ternary Cu- and Sn-based subsystems is crucial for the brazing processes. Thermodynamic properties of binary Sn–Ti and Sn–Zr systems are comparatively fully studied [1–5], but discrepancies between the published assessments still remain, and some aspects are undetermined. In particular the intervals of solubility at higher temperatures, the structure of intermetallic compounds and their thermal expansion, especially near the liquidus line on the Sn rich side of these systems have scarcely been studied.

The components of the Sn–Ti, Sn–Zr and Sn–Ti–Zr systems show substantial differences in their melting temperatures. Therefore, the addition of a refractory element effects a drastic increase in the liquidus line, and even a negligible error in the alloy composition can provoke a serious error in determining the onset of solidification. Because of this peculiarity and the experimental difficulties, the data on structure-sensitive properties of these systems in the liquid state are scarce in the literature.

The determination of the liquidus temperature by differential thermal analysis (DTA) methods is often very complicated and can lead to substantial errors. At this point, investigations by other methods, supplementing each other, enables this determination to a higher degree of consistency.

Recently the electrical conductivity and viscosity investi- EMPA20090138 of some binary Sn–Ti, Sn–Zr and ternary Sn–Ti–Zr liquid alloys were reported [6, 7]. In this work, viscosity, electrical conductivity and X-ray measurements were carried out for liquid Sn–Ti–Zr alloys on the Sn-rich side over a wide temperature range above the liquidus. Special attention was given to the melting–solidification region.

2. Materials and methods

2.1. Materials

A number of ternary Sn–Ti–Zr alloys covering the Sn-rich corner of the phase diagram and providing the most exhaustive information were selected for the studies. The sample compositions are listed in Table 1. The samples were prepared in an arc melting furnace in a purified argon atmosphere. Ingots of tin, titanium and zirconium, all of them with a purity of 99.99 %, were cleaned of oxide films, then mixed and installed in the chamber of the furnace. In order to achieve good homogeneity, the alloys were remelted 5 times.

2.2. Viscosity

The measurements of the dynamic viscosity were carried out using a computer-controlled oscillating-cup viscometer [8]. Cylindrical boron nitride crucibles were used. The temperature was measured with a WRe-5/20 thermocouple arranged just below the crucible. The experiments were performed in an atmosphere of $Ar + H_2$ after initially pumping out the working volume of the furnace to about 10 Pa. A homogeneous temperature field was created inside

Table 1. Reference liquidus temperatures for different Sn–Ti, Sn–Zr [6, 7] and Sn–Ti–Zr alloys.

Composition (at.%)	Reference liquidus temperature T_L (K)	Composition (at.%)	Reference liquidus temperature T_L (K)
$Sn_{98}Ti_2$	681	$Sn_{95}Ti_{2.5}Zr_{2.5}$	730
$Sn_{95}Ti_5$	735	$Sn_{85}Ti_{7.5}Zr_{7.5}$	860
$Sn_{85}Ti_{15}$	880	$Sn_{75}Ti_{12.5}Zr_{12.5}$	1090
$Sn_{75}Ti_{25}$	1095	$Sn_{65}Ti_{17.5}Zr_{17.5}$	1400
$Sn_{65}Ti_{35}$	1420	$Sn_{65}Ti_{26.25}Zr_{8.75}$	1410
$Sn_{55}Ti_{45}$	1675	$Sn_{65}Ti_{8.75}Zr_{26.25}$	1550
$Sn_{98}Zr_2$	702	$Sn_{85}Ti_{4.25}Zr_{10.75}$	990
$Sn_{95}Zr_5$	934	$Sn_{85}Ti_{10.75}Zr_{4.25}$	865
$Sn_{85}Zr_{15}$	1280	$Sn_{75}Ti_{6.25}Zr_{18.75}$	1190
$Sn_{75}Zr_{25}$	1420	$Sn_{75}Ti_{18.75}Zr_{6.25}$	1090
$Sn_{65}Zr_{35}$	1690		

the furnace. The sample was initially heated and held at high temperatures well above the liquidus until the oscillation period did not change any more with time indicating that the sample had become homogeneous. The measurements were carried out several times during heating and cooling in order to get reliable values. Usually the first measurement was carried out with a temperature interval of 10 K in order to estimate the melting–solidification region. The next runs were carried out paying special attention to this region, i.e. when approaching the liquidus the measuring step was reduced to 5 K. The heating and cooling rates were reduced to about 20 K h^{-1}. The resultant error in the viscosity did not exceed 5 %.

2.3. Electrical conductivity

The electrical conductivity was measured by a contact method in accordance with the 4-point scheme as described elsewhere [9]. The samples were contained in measuring cells manufactured from boron nitride ceramics in the form of vertical cylinders with an operating cavity height of 60 mm. The graphite electrodes for the current and potential measurements were inserted into the wall of the container along its vertical axis. The potential electrodes were provided with WRe-5/20 thermocouples. The experiments were performed in an inert atmosphere of argon. The resultant error in the electrical conductivity did not exceed 2 %. Heating and cooling were performed in the same way as described in Section 2.2.

2.4. X-ray diffraction

The X-ray diffraction (XRD) studies were carried out using a high-temperature diffractometer with a special attachment that allows investigation of the solid and liquid samples at different temperatures up to 1600 K. Cu-K_α radiation monochromatized by means of single crystal LiF as a monochromator and Bragg–Brentano focusing geometry were used. The scattered intensities as a function of the scattering angle were recorded within the range 1 $Å^{-1} < k < 7$ $Å^{-1}$, with different angular steps, which were equal to 0.05° within the region of principal peak and 0.5° at the remaining values of wave vectors. The measurement of the scattered intensity was done with high accuracy, better than 2 %. In order to obtain the more accurate scattered intensities, the scan time was equal to 100 s. The diffracted intensity was recorded using an NaI(Tl) scintillated detector in conjunction with an amplification system. The sample was placed in a rounded cup of 20 mm diameter. Scattered intensities as functions of scattering angles were recorded and corrected on absorption, anomalous dispersion and incoherent scattering [10]. The structure factors (SF) were obtained from angular dependences of scattered intensities.

2.5. Microstructure

Microscopic studies of the solidified specimens were performed using a field emission scanning electron microscope (SEM). The specimens were ground and polished as is usually done for metallographic investigations. In addition, energy dispersive X-ray (EDX) measurements were performed in order to determine the local phase compositions of the alloys. The primary phases were carefully analysed in order to determine the solidification sequence.

3. Results and discussion

3.1. Viscosity measurements

The dynamic viscosity, $\eta(T)$, was measured in a wide temperature range above the liquidus. The η values were calculated from the logarithmic decrement between consecutive swings and the period of oscillations, using the modified Roscoe equation, proposed in [11]. It was revealed that the viscosity increases exponentially with cooling and the temperature dependence is rather well described by the Arrhenius equation for all investigated alloys. Admixtures of Ti and Zr increase the viscosity of liquid Sn. As the content of titanium or zirconium increases, the temperature dependence of viscosity becomes weaker.

Taking into account that the logarithmic decrement is more sensitive to different structure transformations than the viscosity itself, we considered the temperature dependence of the logarithmic decrement, $\delta(T)$, for the liquidus determination in the present work. The $\delta(T)$ data for some Sn–Ti–Zr alloys are shown in Fig. 1. The same temperature dependence of the logarithmic decrement was also observed for other investigated alloys.

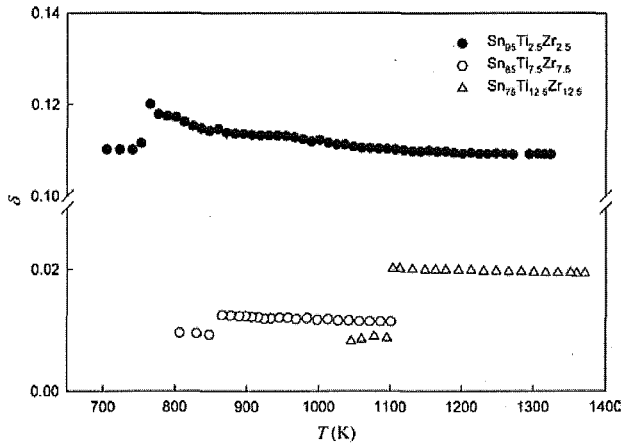

Fig. 1. Logarithmic decrement of liquid Sn–Ti–Zr alloys as a function of temperature.

3.2. Electrical conductivity measurements

It was shown recently that the electrical conductivity, $\sigma(T)$, of the Sn-rich binary Sn–Ti, Sn–Zr and ternary Sn–Ti–Zr alloys decreases gradually with heating and with an increase in the Ti or/and Zr additions [6, 7]. Similar conductivity behaviour is typical for all the alloys, investigated in this study. Some selected $\sigma(T)$dependences are presented in Fig. 2.

In our previous work the conductivity results were interpreted in the context of the s–d hybridization model [6]. The Ti and Zr dopants belong to transition metals with partially filled d shells. The d states in such solutes can be described using the Friedel–Anderson scheme, central to which is the concept of virtual bound states. The electrical conductivity of a liquid alloy is expressed as [12]:

$$\sigma = \frac{n_e e^2 L_0}{\hbar k_f} \tag{1}$$

where n_e is the electron density, e is the electron charge, L_0 is the mean free path of conduction electrons, k_f is the Fermi wave number. The change in conductivity can be attributed to the changes in the parameters n_e and L_0. The later is due to the structure changes, which may include the altering of the nearest neighbour distance, the first coordination number, as well as the relaxation time of s–d resonance scattering. n_e can lead either to an increase or to a decrease in conductivity [13, 14], whereas a decrease in L_0 due to the s–d resonance scattering always results in a decrease in conductivity, as occurs if Ti or Zr are added to liquid Sn (Fig. 2).

Transition from the liquid to the solid state during cooling is accompanied by a rapid increase in the electrical conductivity (Fig. 2), which is specific for each composition, and corresponds to the onset of solidification. Contrary to the abrupt conductivity changes in pure metals during the liquid–solid transition, the extended conductivity increase during solidification is explained by a gradual precipitation of the solid phases between the liquidus and solidus temperatures, which is peculiar to systems with substantial differences between the component melting temperatures.

A detailed analysis and comparison of the logarithmic decrement and electrical conductivity results have made possible the determination of the liquidus temperatures with higher accuracy compared to other methods. As an example, the melting–solidification region of the $Sn_{95}Ti_{2.5}Zr_{2.5}$ liquid alloy is presented in Fig. 3.

As can be seen from Fig. 3a, a drastic decrease in $\delta(T)$ below approximately 733 K indicates the onset of solidification, corresponding to the liquidus temperature, T_L. Similar behaviour of the logarithmic decrement was observed for the other alloys.

Typical temperature dependence of the electrical conductivity is presented in Fig. 3b. In the molten state conductivity decreases with heating and increases with cooling. A kink on the $\sigma(T)$ curve indicates that solidification starts at approximately 730 K (T_L).

The melting–solidification process is usually accompanied by a certain temperature hysteresis of different physical properties. The range of melting can be extended to higher temperatures when heating is rapid. The temperature of the solidification onset T_L during cooling is usually lower than the temperature of the melting completion T_M in the course of heating [6]. T_L depends on the cooling velocity, on the temperature of the overheating, and also on the holding time at highest temperatures (degree of homogeneity). In other words, T_L depends on conditions of crystal nucleation. Depending on sample composition, precipitation of primary crystals could be in the form of intermetallic compounds, which could serve as crystallizing nuclei. Thus, some temperature interval always inheres in the melting–solidification process, and $T_M > T_L$. It should be noted that Fig. 3a and b presents the averaged values obtained in the course of several experimental runs with samples of the same compositions.

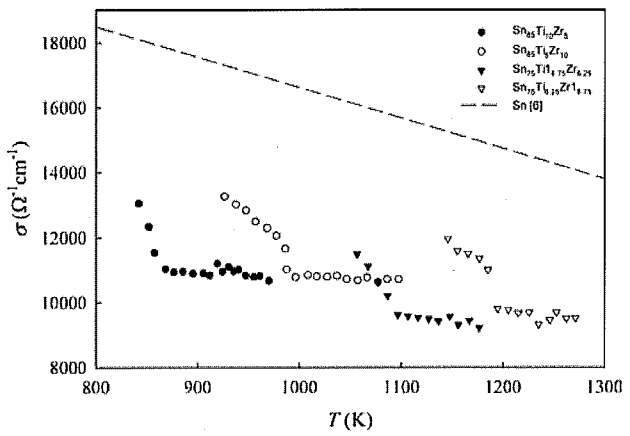

Fig. 2. Electrical conductivity of liquid Sn–Ti–Zr alloys as a function of temperature.

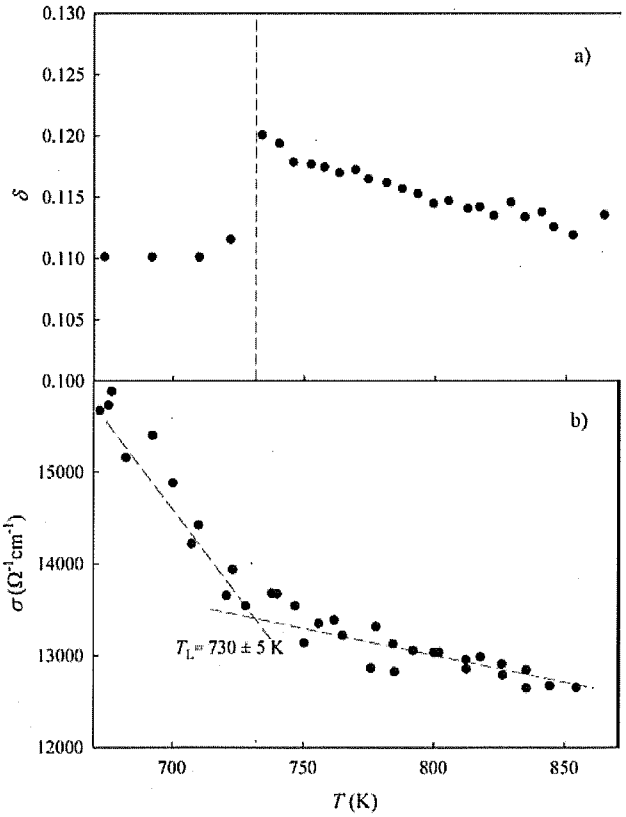

Fig. 3. (a) Logarithmic decrement and (b) electrical conductivity as functions of temperature of the $Sn_{95}Ti_{2.5}Zr_{2.5}$ liquid alloy in the melting-solidification region.

3.3. XRD measurements

The XRD measurements were carried out at three temperature values. The initial temperature, T_1, was set to 5 K above the liquidus determined for each alloy from the electrical conductivity and viscosity experiments. The second temperature, T_2, was 10 K lower, and the third measurement was made at room temperature, T_R. The samples were held at each temperature for 30 min.

As an example, the structure factor (SF) for the liquid $Sn_{95}Ti_{2.5}Zr_{2.5}$ alloy is shown in Fig. 4 (upper curve) and is similar to the SF of liquid tin. The diffraction patterns obtained at T_2 revealed peaks corresponding to the crystalline phases. As the density of the crystallites is lower than the density of the liquid phase, they rise to the surface of the melt. At this point, the temperature at which the crystalline-like peaks appear on the background of the diffraction pattern of the liquid phase can be considered as just a point close to the liquidus temperature. It is clear that the precision of liquidus temperature determination depends on nucleus critical size, whose experimental value is not available at this time. The peaks corresponding to the crystalline phases are very wide due to a small crystallite size. Identification of the peaks, which show a higher resolution at lower temperature (Fig. 4, middle curve) suggests the existence of the solid $ZrSn_2$ and Ti_2Sn_3 phases.

It should be noted that the usual content of these intermetallics is negligible. Their appearance at the diffraction pattern of the solid–liquid mixture (Fig. 4, middle curve) is explained by their preferential location on the surface and hence more significant contribution to the scattered intensity. At room temperature the crystallites are randomly distributed in the tin matrix volume. Therefore, they are not identified, and the diffraction pattern is similar to that of pure tin (Fig. 4, lower curve).

Similar XRD measurements were carried out for other Sn–Ti–Zr alloys. Based on the XRD data both in the liquid and the solid states, it is suggested that at the onset of solidification the influence of structural features of the liquid is significant. The formation tendency of chemically ordered structural units with a structure similar to the structure of intermetallics, suggest the availability of clusters in the liquid (this means only chemical ordering (not topological) due to preferred interaction of different atoms of the different elements in the liquid intermetallic phase). These clusters aggregate into larger structure units, which reach a critical size under equilibrium conditions of solidification and become the nuclei of the solid phase. Just before solidification a melt containing such clusters could be very sensitive to the ambient influence (pressure, uncontrolled impurities, electric and magnetic fields, etc.) and cooling conditions. In some cases the cluster aggregation process can be inhibited resulting in undercooling. But sometimes the cluster formation starts at higher temperatures, and the clusters can exist within a wide temperature range before solidification. Nevertheless, a reduced cooling rate allows determination of the liquidus temperatures T_L with rather high accuracy.

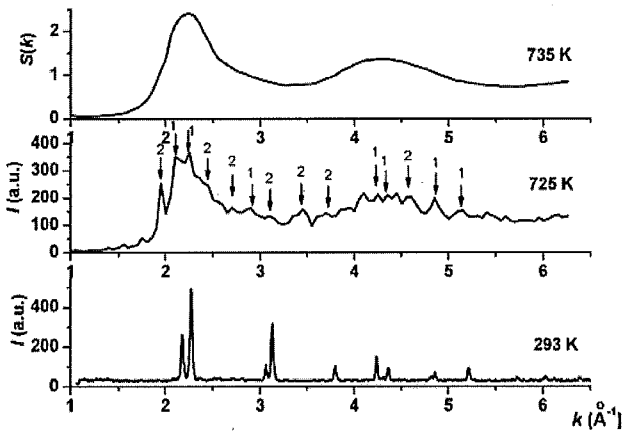

Fig. 4. Structural changes on solidification of $Sn_{95}Ti_{2.5}Zr_{2.5}$ alloy: the upper curve was obtained in the completely liquid state, the curve in the middle was obtained just below the liquidus; the lower curve was obtained at room temperature (1-Sn; 2-$ZrSn_2$, 3-Ti_2Sn_3).

3.4. Microstructures, liquidus projection and reaction scheme

In order to describe the solidification scheme for ternary Sn–Ti–Zr alloys, the microstructures of the solidified specimens were characterized by SEM. In Fig. 5 representative microstructures of four different Sn–Ti–Zr alloys ($Sn_{95}Ti_{2.5}Zr_{2.5}$, $Sn_{75}Ti_{12.5}Zr_{12.5}$, $Sn_{65}Ti_{26.25}Zr_{8.75}$, $Sn_{65}Ti_{8.75}Zr_{26.25}$) after melting and solidification are shown. In comparison with the soft tin matrix, the intermetallic phases are very hard and brittle, resulting in numerous cracks which are visible in the SEM pictures. The different phases as determined by EDX measurements are given in order of formation in Table 2. In the Sn rich specimen $Sn_{95}Ti_{2.5}Zr_{2.5}$ the primary phase was identified as $(Ti, Zr)_2Sn_3$ which is embedded in the Sn matrix (cf. Fig. 5a). $(Zr, Ti)Sn_2$ as the secondary phase was not found, which is most probably because only a very little amount of that phase might be formed. The alloy $Sn_{95}Ti_{7.5}Zr_{7.5}$ showed a very similar microstructure. For the alloy $Sn_{65}Ti_{26.25}Zr_{8.75}$, $(Ti, Zr)_6Sn_5$ was identified as the primary phase. Besides that, $(Ti, Zr)_2Sn_3$ could be detected whereas no $(Zr, Ti)Sn_2$ was found (cf. Fig. 5b). The alloys $Sn_{75}Ti_{12.5}Zr_{12.5}$, $Sn_{65}Ti_{17.5}Zr_{17.5}$, $Sn_{75}Ti_{6.25}Zr_{18.75}$ and $Sn_{75}Ti_{8.75}Zr_{26.25}$, showed similar microstructures with the phases $(Ti, Zr)_6Sn_5$, $(Zr, Ti)Sn_2$ and $(Ti, Zr)_2Sn_3$ in the Sn matrix (cf. Fig. 5c and d). These results correlate well with the above mentioned findings of the XRD measurements and they allowed estimating the extension of the surfaces of primary solidification.

Based on the above mentioned findings, all possible isopleth sections describing the liquidus temperature range

Table 2. Phases in different Sn–Ti–Zr alloys in order of appearance during solidification as detected by SEM/EDX (phases in square brackets could not be observed).

Composition (at.%)	1	2	3	4
$Sn_{95}Ti_{2.5}Zr_{2.5}$	$(Ti, Zr)_2Sn_3$	$[(Zr, Ti)Sn_2]$	Sn	–
$Sn_{85}Ti_{7.5}Zr_{7.5}$	$(Ti, Zr)_2Sn_3$	$[(Zr, Ti)Sn_2]$	Sn	–
$Sn_{75}Ti_{12.5}Zr_{12.5}$	$(Ti, Zr)_6Sn_5$	$(Zr, Ti)Sn_2$	$(Ti, Zr)_2Sn_3$	Sn
$Sn_{75}Ti_{6.25}Zr_{18.75}$	$(Ti, Zr)_6Sn_5$	$(Zr, Ti)Sn_2$	$(Ti, Zr)_2Sn_3$	Sn
$Sn_{65}Ti_{17.5}Zr_{17.5}$	$(Ti, Zr)_6Sn_5$	$(Zr, Ti)Sn_2$	$(Ti, Zr)_2Sn_3$	Sn
$Sn_{65}Ti_{26.25}Zr_{8.75}$	$(Ti, Zr)_6Sn_5$	$[(Zr, Ti)Sn_2]$	$(Ti, Zr)_2Sn_3$	Sn
$Sn_{65}Ti_{8.75}Zr_{26.25}$	$(Ti, Zr)_6Sn_5$	$(Zr, Ti)Sn_2$	$(Ti, Zr)_2Sn_3$	Sn

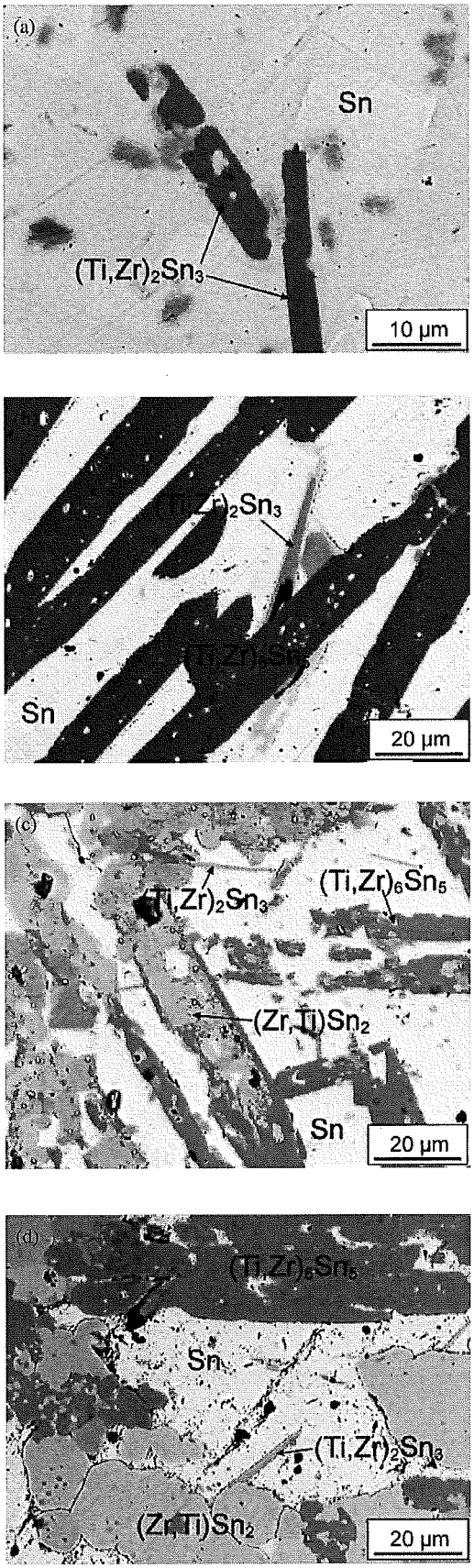

Fig. 5. Characteristic microstructures of Sn–Ti–Zr alloys; (a) $Sn_{95}Ti_{2.5}Zr_{2.5}$, (b) $Sn_{75}Ti_{12.5}Zr_{12.5}$, (c) $Sn_{65}Ti_{26.25}Zr_{8.75}$ (d) $Sn_{65}Ti_{8.75}Zr_{26.25}$.

were derived. Figure 6 shows as an example the measured liquidus temperatures as a function of the Zr content for different constant Sn contents. Similar plots were obtained for the alloys with Ti:Zr ratios of 3:1, 1:1 and 1:3, respectively, and varying Sn contents. Isotherms in the ternary Sn–Ti–Zr system could then be determined from the interpolated curves as well as from the available data for the binary alloys [5]. Figure 7 shows the proposed liquidus projection of the Sn–Ti–Zr system on the Sn-rich side displaying the surfaces of primary solidification as observed in the melted and solidified samples. The positions of the invariant reactions U_1: $L + (Ti, Zr)_5Sn_3 \leftrightarrow (Ti, Zr)_6Sn_5 + (Zr, Ti)Sn_2$ and U_2: $L + (Ti, Zr)_6Sn_5 \leftrightarrow (Ti, Zr)_2Sn_3 + (Zr, Ti)Sn_2$ were estimated according to the above mentioned findings. Based on the liquidus surfaces for primary solidification the possible solidification scheme was de-

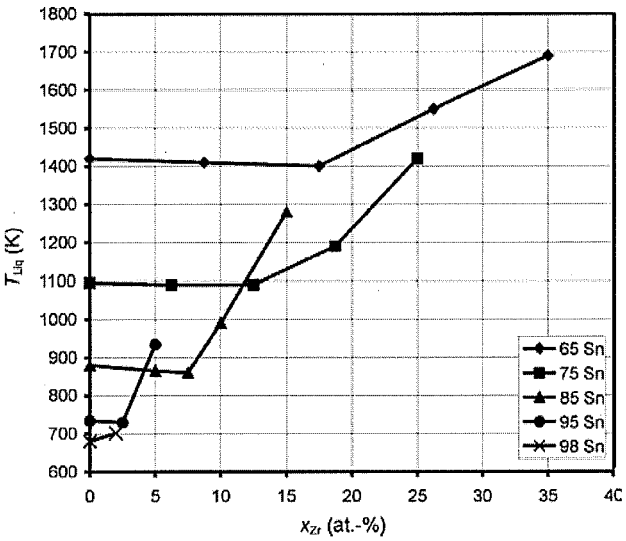

Fig. 6. Liquidus temperature as a function of Zr content for different constant Sn contents.

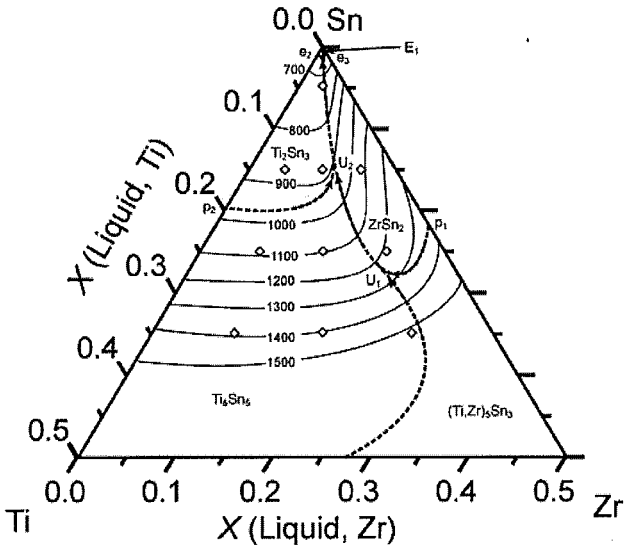

Fig. 7. Proposed liquidus projection of Sn–Ti–Zr system in the Sn-rich corner based on the current measurements (e_3, e_4, e_5: binary eutectic reactions, p_3, p_4: binary peritectic reactions, E_1: ternary eutectic reaction, U_1, U_2: ternary quasi-peritectic reactions).

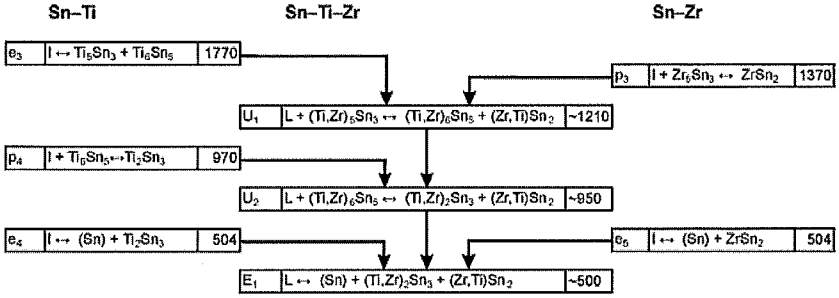

Fig. 8. Partial reaction scheme of the Sn–Ti–Zr system in the Sn rich corner, T in K.

rived and is presented in Fig. 8. The temperatures of the binary reactions were taken from [5]. The temperatures of the ternary reactions of approximately 950 K for U_1 and approximately 1210 K for U_2 were estimated from the liquidus projection. However, a more precise characterization of these reactions would require additional tests, which were beyond the scope of this work. Even if only a small number of experiments were performed, they offer a first description of the Sn rich part of the Sn–Ti–Zr system.

4. Summary

The liquidus temperatures of the Sn–Ti–Zr liquid alloys were determined from viscosity, electrical conductivity and XRD experiments. Based on repeated measurements for each composition and the results obtained, the confidence intervals of liquidus temperatures were determined. This confidence interval, which is inevitable in systems with substantial differences between the component melting temperatures, includes different values of the liquidus temperatures determined by different experimental methods. The recommended values for liquidus temperatures for binary Sn–Ti, Sn–Zr (taken from [6, 7]) and ternary Sn–Ti–Zr alloys are collected in Table 1. Based on these data, the liquidus projection of Sn–Ti–Zr system in the Sn-rich corner as well as the possible solidification scheme was determined.

This work was financially supported by Swiss National Science Foundation (SNF) in the framework of the SCOPES research project No. IB7320-111101/1.

References

[1] N. Dupin, I. Ansara, C. Servant, C. Toffolon, C. Lemaignan, J.C. Brachet: J. Nucl. Mater. 275 (1999) 287.
[2] N. Subasic: Calphad 22 (1998) 157.
[3] C. Liu, U.E. Klotz, P.J. Uggowitzer, J.F. Löffler: Monatsh. Chem. 136 (2005) 1921.
[4] F. Yin, J.C. Tedenac, F. Gascoin: Calphad 31 (2007) 370.
[5] C. Liu: Characterisation and Modelling of Interface Reactions between Diamond and Active Brazing Alloys. Ph.D. Thesis No. 17469. ETH Zuerich, 2007.
[6] Y. Plevachuk, S. Mudry, V. Sklyarchuk, A. Yakymovych, U.E. Klotz, M. Roth: J. Mater. Sci. 42 (2007) 8618.
[7] V. Sklyarchuk, Y. Plevachuk, S. Mudry, A. Yakymovych, U.E. Klotz, C. Liu: J. Phys.: Conf. Series 98 (2008) 062008.
[8] S. Mudry, V. Sklyarchuk, A. Yakymovych: J. Phys. Studies. 12 (2008) 1601.
[9] Y. Plevachuk, V. Sklyarchuk: Meas. Sci. Technol. 12 (2001) 23.
[10] D.T. Cromer, J.T. Waber: Acta Cryst. 18 (1965) 104.
[11] J. Vollmann, D. Riedel: J. Phys.: Condens. Matter 8 (1996) 6175.
[12] T.E. Faber: An introduction to the theory of liquid metals, Cambridge Univ., London (1972).
[13] S. Ohno, S. Harada: J. Phys. Soc. Jpn. 49 (1980) 189.
[14] S. Mudry, V. Sklyarchuk, Y. Plevachuk, I. Shtablavyi: Inorg. Mater. 44 (2008) 129.

(Received May 13, 2008; accepted October 25, 2008)

Bibliography

DOI 10.3139/146.110086
Int. J. Mat. Res. (formerly Z. Metallkd.)
100 (2009) 5; page 689–694

ISSN 1862-5282

Correspondence address

Dr. Y. Plevachuk
Ivan Franko National University
Department of Metal Physics
8, Kyrylo and Mephodiy Str., 79005 Lviv, Ukraine
Tel.: +38 032 239 4270
Fax: +38 032 295 6908
E-mail: plevachuk@mail.lviv.ua